Electronic band structure and structural stability of LaBiPt

Tamio Oguchi
Department of Quantum Matter, Graduate School of Advanced Sciences of Matter (ADSM), Hiroshima University, Higashihiroshima 739-8526, Japan

(Received 27 October 2000; published 13 March 2001)

The electronic structure and structural stability of LaBiPt are studied by using relativistic local-density energy band calculations. Total-energy calculations for three different atomic configurations within the MgAgAs-type crystal structure show that the Pt atom is definitely on a unique site. For the stable configuration, LaBiPt is semimetallic with hole and electron carrier concentrations of $10^{-4}e$. Calculated hole Fermi surfaces have nearly a cubic shape, whose cross sections and their field-angle dependence are in good agreement with recently observed Shubnikov–de Haas result. LaBiPt becomes a zero-gap semiconductor without the spin-orbit coupling, indicating that LaBiPt is a spin-orbit induced semimetal. The semimetallic nature originates mostly in BiPt and may be inherent in wider material systems like *R*BiPt with rare-earth elements *R*.

DOI: 10.1103/PhysRevB.63.125115 PACS number(s): 71.20.Gj, 71.18.+y, 61.66.Dk

I. INTRODUCTION

Ternary intermetallic compounds *R*BiPt [*R*=rare earth (RE) metals except Pm and Eu, La, and Y] are known to be small-gap semiconductors or semimetals while YbBiPt and LuBiPt are metals.[1] *R*BiPt (*R*=RE) shows antiferromagnetic order with Néel temperatures of a few degrees. The most striking feature in the series is that YbBiPt is a superheavy fermion system with a linear coefficient of specific heat of 8 J/K^2, which is the largest among the known heavy fermions.[2] *R*BiPt has cubic MgAgAs crystal structure, often called the half-Heusler structure. The lattice constants change from 6.87 Å (La) to 6.59 Å (Lu) in the series.[1] In the MgAgAs structure, internal atomic coordinates are (1/4,1/4,1/4) for Mg, (0,0,0) for Ag, and (3/4,3/4,3/4) for As and, thus, the Ag atom is located on the unique site. Until 1994, it has been believed that the Bi atom is on the unique site at least for *R*BiPt with the heaver RE atoms. Robinson *et al.*[3] have concluded that the Pt atom is on the unique site in YbBiPt by neutron diffraction experiments. Low-temperature transport properties of NdBiPt have been studied by Morelli *et al.*[4] By analyzing the temperature dependence of longitudinal resistivity and Hall resistivity within a two-carrier model, a semimetallic electronic structure with a very small overlap of valence (hole) and conduction (electron) bands is concluded.

Electronic structure calculations for the *R*BiPt systems have been reported by Eriksson *et al.*,[5] McMullan and Ray,[6] and Oppeneer *et al.*[7] Eriksson *et al.* have calculated the electronic structure of YBiPt and YbBiPt by using the fully relativistic linear muffin-tin orbital (LMTO) method within the local-density approximation (LDA) with assumption of the Bi atom on the unique site. McMullan and Ray have also calculated the band structure of YbBiPt by the LMTO method with Bi on the unique site and discussed detailed Fermi surface topology. Oppeneer *et al.* have applied the LDA approach generalized with additional intra-atomic Coulomb correlations between the 4*f* electrons (LDA+*U*) to YbBiPt with Pt on the unique site and found extremely narrow 4*f* states pinned at the Fermi energy (ε_F) to give rise to a very large specific heat. It might be useful to cite a related electronic structure study by Öğüt and Rabe,[8] who have calculated the electronic structure and total energy for *M*NiSn (*M*=Ti,Zr,Hf) with the same half-Heusler structure as *R*BiPt and discussed the structural stability and the origin of energy gaps.

In order to investigate the electronic properties of *R*BiPt, it is very important to study the electronic structure of LaBiPt as a basic f^0 electronic system. Quite recently, Jung *et al.*[9] have measured electric resistivity, Hall coefficient, and thermal conductivity for LaBiPt and found that LaBiPt is a semimetal with a hole concentration of $+0.00035e$ per formula unit as a dominant carrier. Goll *et al.*[10] have discovered superconductivity at 0.88 K in LaBiPt. They also have observed Shubnikov–de Haas (SdH) oscillations in the electric resistivity measurement at low temperatures and found a simple and very small Fermi surface. The obtained Fermi surface cross sections are 65 T, 93 T, and 95 T for the field angles of [001], [111], and [110] directions, respectively. Assuming a cubic Fermi surface with a dimension of only 8.6% of of ΓX distance of the face-centered-cubic (fcc) Brillouin zone, one can estimate the corresponding cross sections of 65 T, 85 T, and 92 T. Therefore, the observed cross sections may originate in such a very small cubic Fermi surface. Considering the results of the Hall and thermal resistivity measurements,[9] the Fermi surface may be a hole surface. In addition to the hole Fermi surfaces, there must be some small electron surfaces to compensate the hole carriers.

In the present paper, the structural stability and electronic structure of LaBiPt are studied by means of a first-principles method within LDA. Total-energy calculations are carried out as a function of the unit-cell volume for three different atomic configurations in the cubic MgAgAs crystal structure, namely either La, Bi, or Pt on the unique site. The total-energy result shows that the Pt is definitely on the unique site and the equilibrium lattice constant evaluated is in excellent agreement with experiment within error of 0.7%. LaBiPt with the stable configuration is semimetallic with very small hole and electron Fermi surfaces, whose volume is only order of 10^{-2} of the Brillouin zone. Quite strikingly, it is found that such a semimetallic behavior disappears without the spin-orbit coupling (SOC).

II. METHODS

Electronic structure and total-energy calculations are performed with all-electron full-potential linear augmented plane wave (FLAPW) method[11–13] with an iterative scheme.[14] Scalar-relativistic self-consistent-field Kohn-Sham equations are solved as

$$\mathcal{H}\psi^{\mathbf{k}}_{i,\sigma}(\mathbf{r})=\left[-\frac{\hbar^2}{2m}\nabla^2+v^{\sigma}_{\mathrm{eff}}(\mathbf{r})\right]\psi^{\mathbf{k}}_{i,\sigma}(\mathbf{r})=\varepsilon^{\mathbf{k}}_{i,\sigma}\psi^{\mathbf{k}}_{i,\sigma}(\mathbf{r}), \tag{1}$$

where $v^{\sigma}_{\mathrm{eff}}(\mathbf{r})$ is the Kohn-Sham effective potential for spin σ and $\varepsilon_{i,\sigma}$ and $\psi^{\mathbf{k}}_{i,\sigma}(\mathbf{r})$ are the eigenvalue and wave function to be solved. Fully relativistic Bloch wave functions are thus given in terms of the scalar-relativistic wave functions as

$$\Psi^{\mathbf{k}}_{n}(\mathbf{r})=\sum_{i,\sigma}\psi^{\mathbf{k}}_{i,\sigma}(\mathbf{r})C_{i,\sigma,n} \tag{2}$$

where the expansion coefficients $C_{i,\sigma,n}$ are determined variationally by diagonalizing the Hamiltonian matrix including SOC $\mathcal{H}_{\mathrm{SOC}}$ (second variation[15])

$$[\mathcal{H}+\mathcal{H}_{\mathrm{SOC}}]\Psi^{\mathbf{k}}_{n}(\mathbf{r})=\mathcal{E}^{\mathbf{k}}_{n}\Psi^{\mathbf{k}}_{n}(\mathbf{r}) \tag{3}$$

with the fully relativistic eigenvalues $\mathcal{E}^{\mathbf{k}}_{n}$. Our all-electron fully relativistic iterative FLAPW approach has been successfully applied to various kinds of transition-metal and actinide systems.[16–18]

Self-consistency is attained by adopting $8\times8\times8$ uniform k-point sampling with the improved tetrahedron method of Blöchl *et al.*[19] and the plane-wave cutoff of $RK_{\max}=8.5$. In the second-variation procedure, states up to 2 Ry above ε_{F} are included in the expansion [Eq. (2)]. The number of k points is then increased up to $20\times20\times20$ and calculated eigenvalues are fitted to a star-function expansion[20] by a least-squares method to obtain accurate geometry of very small Fermi surface.

III. RESULTS AND DISCUSSION

A. Structural stability

As mentioned above, there are three fcc sublattices in the MgAgAs structure, i.e., Mg(1/4,1/4,1/4), Ag(0,0,0), and As(3/4,3/4,3/4). The Mg and As atomic sites are coordinated tetrahedrally by four nearest-neighbor Ag while the Ag site doubly tetrahedrally by four Mg and four As. Therefore, the Ag site can be regarded as the unique site in the crystal structure. Total-energy calculations for LaBiPt have been carried out for three kinds of atomic configurations, La, Bi, or Pt on the unique site, as a function of unit-cell volume (V) in order to determine theoretical equilibrium crystal structure. Calculated total energies are plotted in Fig. 1.

The total energies $E(V)$ are then least-squares-fitted to Murnaghan's equation of state[21]

$$E(V)=\frac{B_0V}{B_0'}\left[\frac{(V_0/V)^{B_0'}}{B_0'-1}+1\right]+\mathrm{const}, \tag{4}$$

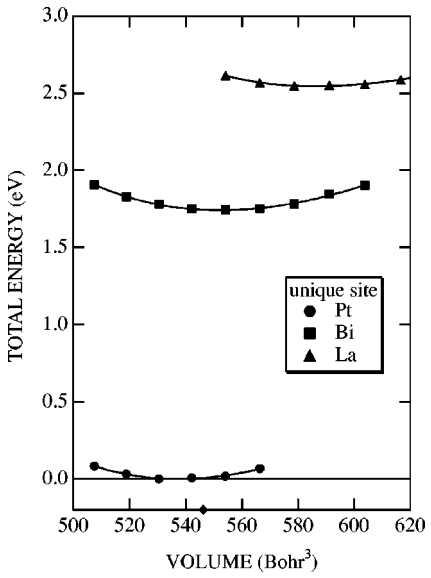

FIG. 1. Calculated total energies per formula unit for LaBiPt with different atomic configurations, La (triangles), Bi (squares), or Pt (bullets) on the unique site, in the MgAgAs crystal structure as a function of unit-cell volume. The total energies are relative to the minimum one of the most stable configuration. Lines are least-squares-fitted curves to Murnaghan's equation of state [Eq. (4)]. A diamond on the horizontal axis represents the experimental equilibrium volume at 300 K taken from Ref. 9.

where B_0 and B_0' are the bulk modulus and its pressure derivative at the equilibrium volume V_0. Calculated lattice constants, bulk moduli and minimum total energies are listed in Table I for the three atomic configurations.

As shown in Fig. 1 and Table I, the Pt atom is definitely on the unique site and the configuration with Bi or La on the unique site is much higher in energy. This result is quite consistent with the neutron diffraction study for YbBiPt.[3] Since the scattering cross sections of Bi ($Z=83$) and Pt ($Z=78$) to x rays seem to be almost equivalent, it is hard to distinguish the Bi and Pt sites unambiguously only with the x-ray data. Placing Pt on the unique site in LaBiPt is also reasonable when we see the stable structure of MgAgAs and MNiSn (M=Ti,Zr,Hf),[8] where the small transition-metal atom occupies commonly the unique site. Concerning the stable crystal structure, therefore, LaBiPt can be regarded as a hybrid compound of LaBi with NaCl structure (ionic cohesion), and LaPt and PtBi with zinc-blende structure (covalent cohesion).

TABLE I. Equilibrium lattice constants (a), bulk moduli (B_0), their pressure derivatives (B_0'), and minimum total energies per formula unit relative to that of the most stable structure (ΔE) calculated for LaBiPt with La, Bi, or Pt on the unique site. The experimental lattice constant is measured at 300 K from Ref. 9.

Unique site	a (Å)	B_0 (GPa)	B_0'	ΔE (eV)
La	7.03	70	9.4	2.54
Bi	6.89	85	3.8	1.74
Pt	6.83	99	4.4	0
Expt.	6.867			

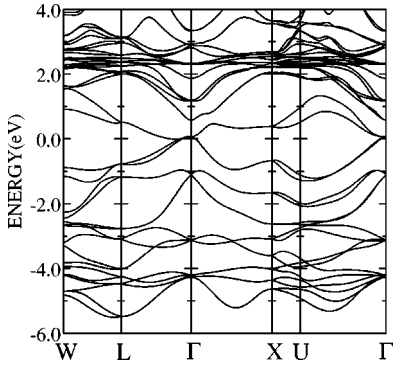

FIG. 2. Calculated fully relativistic energy band structure of LaBiPt along the high-symmetry lines of the fcc Brillouin zone. The calculation has been carried out at the experimental lattice constant $a=6.867$ Å with Pt on the unique site. The Fermi energy is taken at the origin of the energy.

B. Band structure

Fully relativistic energy band structure of LaBiPt with Pt on the unique site and the experimental lattice constant $a=6.867$ Å is shown in Fig. 2. Figure 3 shows the corresponding total density of states in a wider energy range.

As a general characteristic in the band structure, it may be noted that the valence bands are composed mostly of Bi *p* and Pt *d* states slightly mixed with La *d* and *f* states. A Bi *s* band is located just below the valence bands between -11 and -12 eV (not shown in Fig. 2). La *f* states form very narrow unoccupied bands from $+2$ to $+3$ eV above ε_F. The bottom of the conduction bands is made of a mixture of Bi *s* and *p*, Pt *d*, and La *d* and *f* states. The most striking feature seen in Fig. 2 is the semimetallic nature of the band structure. The very low density in the valence and conduction bands around the Fermi energy in Fig. 3 reflects such semimetallic nature. To see more details of the band structure near ε_F, an enlarged band structure is drawn in Fig. 4.

Two valence bands make very small hole pockets around the Γ point and two electron bands make even smaller elec-

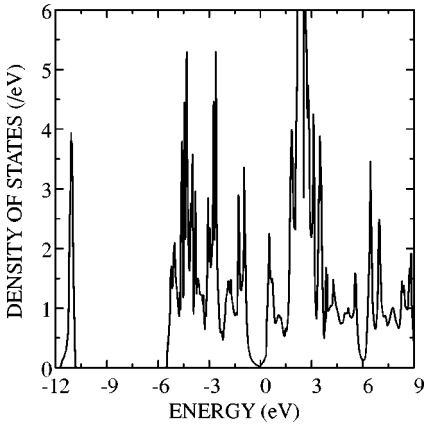

FIG. 3. Calculated fully relativistic density of states of LaBiPt. The unit is states/(eV unit cell spin). The calculation has been carried out at the experimental lattice constant $a=6.867$ Å with Pt on the unique site. The Fermi energy is taken at the origin of the energy.

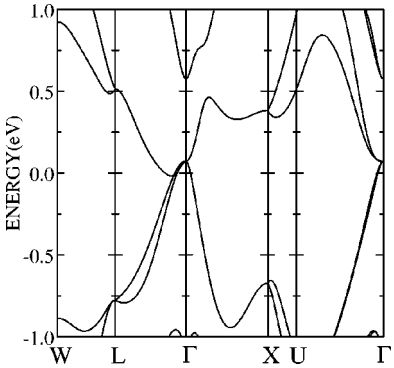

FIG. 4. An enlargement of the fully relativistic energy band structure of LaBiPt near the Fermi energy. The Fermi energy is taken at the origin of the energy.

tron pockets along Λ lines between Γ and *L*. Since the number of electron and hole carriers associated with these Fermi surfaces should be compensated, the average volume of the electron Fermi surfaces is 1/8 that of the hole surfaces. Further discussion on the Fermi surface will be given in next subsection.

In order to clarify the origin of the semimetallic band structure, the SOC is turned off in the calculations, i.e., the second variation process is excluded, and the resulting energy band structure near ε_F is given in Fig. 5. Surprisingly, without the SOC the energy band structure of LaBiPt is of a zero gap semiconductor and the semimetallic behavior disappears completely as shown in Fig. 5. The zero-gap is not accidental and originates from symmetry since the relevant states are triply degenerate without the SOC. This type of the zero-gap band structure is also very peculiar and interesting and may be possibly realized with lighter elements replacing for Bi and/or Pt.

It is worthwhile to mention that the band structure of LaBiPt with Bi on the unique site reveals quite a similar semimetallic behavior to that with Pt on the unique site, as already pointed out by Oppeneer *et al.*[7] This indicates important consequences that the semimetallic feature of the band structure is determined mainly by BiPt with the zinc- blende structure, and that the La states participate in the band structure additively. In the compound formation of LaBiPt, of

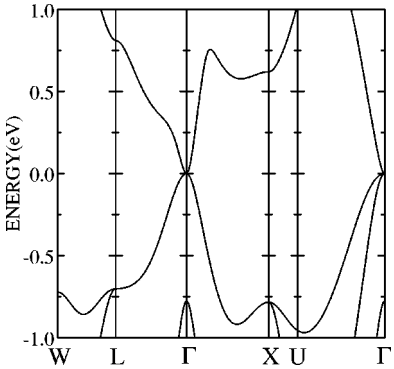

FIG. 5. An enlargement of scalar relativistic energy band structure of LaBiPt near the Fermi energy. The Fermi energy is taken at the origin of the energy.

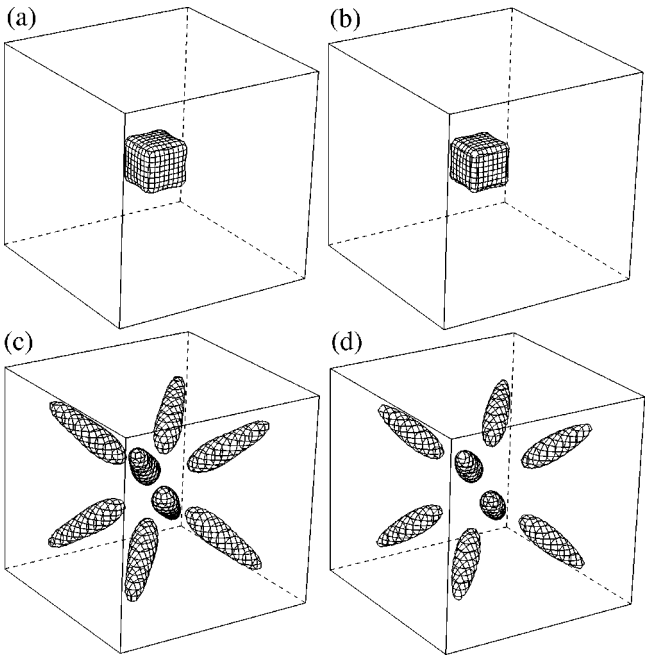

FIG. 6. Calculated Fermi surfaces of LaBiPt: (a) and (b) hole surfaces and (c) and (d) electron surfaces. The Γ point is placed at the center of the box. The dimension of the cubic box is taken to be 1/2 of the Γ*X* distance of the fcc Brillouin zone and then its volume is 1/32 of the full zone.

course, the atomic position of La is crucial as shown in the previous section. Therefore, the basic features seen in LaBiPt are rather common in *R*BiPt systems, and the band structure may be further modified more or less by the different lattice constant and the existence of *f* electrons. Almost equivalent semimetallic band structure to LaBiPt has been speculated from the transport measurements in NdBiPt.[4] Meanwhile, the band structure of LaBiPt with La on the unique site is metallic and totally different from that with Pt or Bi on the unique site.

C. Fermi surface

By inspecting the fully relativistic band structure near ε_F in Fig. 4, there are four kinds of Fermi surfaces, two of which are hole surfaces and the other two are electron ones. Since the electron surfaces are located along Λ lines from Γ to *L*, there exist eight surfaces per one kind, which may have a cigarlike shape. The actual topology of the Fermi surfaces is shown in Fig. 6.

Note that the Fermi surfaces drawn in Fig. 6 are greatly magnified for visual clarity. Two hole surfaces are almost cubelike with concave faces and nearly the same volume. The dimension of the cubic Fermi surfaces is about 20% of the box size, i.e., about 10% of the Γ*X* distance, which is almost comparable with the Fermi surface observed by the SdH measurement.[10] The field-angle dependence of the SdH frequencies corresponds to extremal cross sections of the Fermi surfaces perpendicular to the field. The angle dependence of the extremal cross sections of the hole Fermi surfaces is plotted in Fig. 7 together with experimental data.[10]

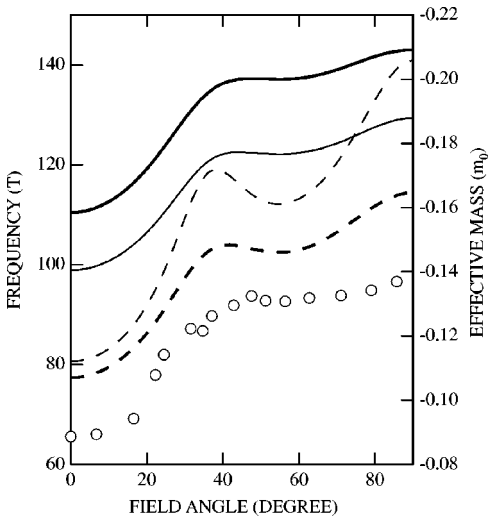

FIG. 7. Calculated SdH frequencies of the hole Fermi surfaces of LaBiPt with low-temperature experimental data (circles) taken from Ref. 10. Thin and thick solid lines denote the frequencies (left axis) calculated for the hole Fermi surfaces of (a) and (b) in Fig. 6, respectively. Thin and thick broken lines represent the corresponding effective cyclotron masses in the free-electron mass unit (right axis). The negative mass means that of hole carriers.

The predicted hole Fermi surfaces have exactly the same topology as the observed one although the absolute value of the cross sections is overestimated by 20–30 %. Considering the smallness of the Fermi surfaces, such agreement is excellent. The hole surfaces contain carriers of $+0.00026e$ and $+0.00022e$. The hole carrier number predicted from the Fermi surfaces is of the same order as the concentration derived from the Hall measurement.[9] The effective cyclotron mass is also evaluated and shown in Fig. 7. The calculated band masses reveal a similar angle dependence to that of the cross sections, varying from $0.11m_0$ to $0.21m_0$, where m_0 is the free-electron mass. The experimental cyclotron mass to be compared has not been reported for LaBiPt though the calculated value can be compared with that of CeBiPt ($0.24m_0$), of which the Fermi surface is almost the same in size.[10]

As for the electron Fermi surface, two sets of eight cigarlike surfaces can be seen in Figs. 6(c) and 6(d). The first set contains $-0.00030e$ carriers while the second one has $-0.00018e$. The cross sections of the electron surfaces are found to be much less than those of the hole surfaces and might be invisible in the SdH measurements.[10] It is very imteresting that the cyclotron mass of the electron orbits is much lighter (at most $0.08m_0$) than that of the hole orbits. Within the constant-relaxation-time approximation (CRTA), the electron and hole carrier mobilities μ_e and μ_h are given as

$$\mu_e = \frac{e\tau_e}{m_e}, \tag{5}$$

$$\mu_h = \frac{e\tau_h}{m_h}. \tag{6}$$

Morelli *et al.*[4] have obtained from transport measurements in semimetallic NdBiPt that the electron mobility is about twice as large as the hole mobility. They have assumed the hole concentration to be larger than the electron concentration due to *p*-type doping (or imperfection) to explain the temperature dependence of the Hall resistivity, which goes from positive (hole dominant) to negative (electron dominant) as the increasing temperature. In the present LaBiPt, the Hall resistivity is all positive in the experimental temperature range (0–300 K) and its value decreases as temperature rises.[9] To make any conclusive statements on the transport properties of LaBiPt, further experimental and theoretical efforts are necessary. Along such lines, we have tried to evaluate the Hall coefficients within the CRTA by calculating the second derivatives of the energy bands on the Fermi surfaces,[22,23] but it turns out to be quite hard to get convergence with respect to the numbers of *k* points and fitting star functions because of very small compensated Fermi surfaces. A total working of band structure calculations, band fitting, and integrations on the Fermi surfaces is needed to attain a highly accurate description of such semimetallic band structure.

IV. CONCLUSIONS

Structural stability and electronic structure of LaBiPt have been investigated by using the all-electron relativistic FLAPW method within LDA. Total-energy calculations for three different atomic configurations in the cubic MgAgAs crystal structure show that the Pt is definitely on the unique site and the theoretical equilibrium lattice constant is in excellent agreement with experiment within an error of 0.7%. LaBiPt is semimetallic with very small hole and electron Fermi surfaces. The hole Fermi surface topology is quite consistent with a recently observed SdH experiment. The most interesting finding is that the semimetallic behavior disappears without the SOC and originates mainly in the electronic structure of BiPt with the zinc-blende structure. Therefore, the basic features of the energy band structure of LaBiPt may be rather common even in other systems such as *R*BiPt.

ACKNOWLEDGMENTS

The author would like to thank T. Takabatake, M. H. Jung, K. Terakura, T. Jo, and T. Shishidou for invaluable discussions.

[1] P. C. Canfield, J. D. Thompson, W. P. Beyermann, A. Lacerda, M. F. Hundley, E. Peterson, Z. Fisk, and H. R. Ott, J. Appl. Phys. **70**, 5800 (1991).
[2] Z. Fisk, P. C. Canfield, W. P. Beyermann, J. D. Thompson, M. F. Hundley, H. R. Ott, E. Felder, M.B. Maple, M. A. Lopez dela Torre, P. Visani, and C. L. Seaman, Phys. Rev. Lett. **67**, 3310 (1991).
[3] R. A. Robinson, A. Purwanto, M. Kohgi, P. C. Canfield, T. Kamiyama, T. Ishigaki, J. W. Lynn, R. Erwin, E. Peterson, and R. Movshovich, Phys. Rev. B **50**, 9595 (1994).
[4] D. T. Morelli, P. C. Canfield, and P. Drymiotis, Phys. Rev. B **53**, 12 896 (1996).
[5] O. Eriksson, J. M. Wills, and A. M. Boring, J. Alloys Compd. **185**, 145 (1992).
[6] G. J. McMullan and M. P. Ray, J. Phys.: Condens. Matter **4**, 7095 (1992).
[7] P. M. Oppeneer, V. N. Antonov, A. N. Yaresko, A. Ya. Perlov, and H. Eschrig, Phys. Rev. Lett. **78**, 4079 (1997).
[8] S. Öğüt and K. M. Rabe, Phys. Rev. B **51**, 10 443 (1995).
[9] M. H. Jung, T. Yoshino, S. Kawasaki, T. Pietrus, Y. Bando, T. Suemitsu, M. Sera, and T. Takabatake, J. Appl. Phys. (unpublished).
[10] G. Goll, J. Hagel, H. v. Löhneysen, T. Pietrus, S. Wanka, J. Wosnitza, T. Yoshino, and T. Takabatake, cond-mat/0003329 (unpublished).
[11] E. Wimmer, H. Krakauer, M. Weinert, and A. J. Freeman, Phys. Rev. B **24**, 864 (1981).
[12] M. Weinert, E. Wimmer, and A. J. Freeman, Phys. Rev. B **26**, 4571 (1982).
[13] H. J. F. Jansen and A. J. Freeman, Phys. Rev. B **30**, 561 (1984).
[14] J. M. Soler and A. R. Williams, Phys. Rev. B **40**, 1560 (1989).
[15] D. D. Koelling and B. N. Harmon, J. Phys. C **10**, 3107 (1977).
[16] K. Iwashita, T. Oguchi, and T. Jo, Phys. Rev. B **54**, 1159 (1996).
[17] H. Miyazawa and T. Oguchi, J. Magn. Magn. Mater. **192**, 325 (1999).
[18] T. Shishidou and T. Oguchi, Phys. Rev. B **62**, 11 747 (2000).
[19] P. E. Blöchl, O. Jepsen, and O. K. Andersen, Phys. Rev. B **49**, 16 223 (1994).
[20] J. B. Ketterson, F. M. Mueller, and L. R. Windmikker, Phys. Rev. **186**, 656 (1969).
[21] F. D. Murnaghan, Proc. Natl. Acad. Sci. USA **30**, 244 (1944).
[22] T. P. Beaulac, F. J. Pinski, and P. B. Allen, Phys. Rev. B **23**, 3617 (1981).
[23] T. Oguchi and T. Sasaki, J. Phys. Chem. Solids **53**, 1525 (1992).